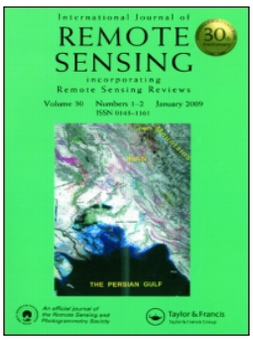

International Journal of Remote Sensing

ISSN: 0143-1161 (Print) 1366-5901 (Online) Journal homepage: http://www.tandfonline.com/loi/tres20

Prediction of daily sea surface temperature using artificial neural networks

S. G. Aparna, Selrina D'Souza & N. B. Arjun

To cite this article: S. G. Aparna, Selrina D'Souza & N. B. Arjun (2018) Prediction of daily sea surface temperature using artificial neural networks, International Journal of Remote Sensing, 39:12, 4214-4231

To link to this article: https://doi.org/10.1080/01431161.2018.1454623

Published online: 23 Mar 2018.

INTERNATIONAL JOURNAL OF REMOTE SENSING, 2018
VOL. 39, NO. 12, 4214–4231
https://doi.org/10.1080/01431161.2018.1454623

Taylor & Francis
Taylor & Francis Group

Prediction of daily sea surface temperature using artificial neural networks

S. G. Aparna[a], Selrina D'Souza[a,b] and N. B. Arjun[a,c]

[a]CSIR-National Institute of Oceanography, Dona Paula, Goa, India; [b]Department of Electronics and Communications Engineering, Manipal Institute of Technology, Udupi, Karnataka, India; [c]IBS Center for Climate Physics and Department of Climate System, Pusan National University, Pusan, South Korea

ABSTRACT

We present an artificial neural network model to predict the sea surface temperature (SST) and delineate SST fronts in the northeastern Arabian Sea. The predictions are made one day in advance, using current day's SST for predicting the SST of the next day. The model is used to predict the SST map for every single day during 2013–2015. The results show that more than 75% of the time the model error is ≤ ±0.5°C. For the years 2014 and 2015, 80% of the predictions had an error ≤±0.5°C. The model performance is dependent on the availability of data during the previous days. Thus during the summer monsoon months, when the data availability is comparatively less, the errors in the prediction are slightly higher. The model is also able to capture SST fronts.

ARTICLE HISTORY
Received 1 September 2017
Accepted 9 March 2018

1. Introduction

Satellite data is very useful in applications, where extensive spatial information is needed, for example, in the field of oceanography, where observations over the sea are sparse, difficult, and expensive. Satellite oceanography gives a wide synoptic coverage at fine spatial detail and the repeated regular sampling helps in generating a long time series that can be used for various applications. For example, for the past few decades, the Indian National Centre for Ocean Information Services (ESSO-INCOIS, Hyderabad, India) used satellite data of sea surface temperature (SST) and phyll to give potential fishing zones (PFZs) advisories (Solanki et al. 2001; Solanki et al. 2005; Zainuddin, Saitoh, and Saitoh 2004). PFZs are thin curves, highlighting the locations where SST fronts (a narrow region of enhanced horizontal gradient of temperature) or SST filaments (narrow elongated regions surrounded by water with different properties) are collocated with higher chlorophyll. The SST fronts and PFZs for a few days are shown in the Figure 1(b,c). The width of these small/mesoscale features is in the order of a few kilometres. Deshpande, Radhakrishnan, and Bhat (2011) showed that a location (on a line parallel to PFZ) about 8–10 km away from the PFZ is considered as non-PFZ region. A recent study by Vipin et al. (2015) showed that the width of an SST filament is about

CONTACT S. G. Aparna aparna@nio.org CSIR-National Institute of Oceanography, Dona Paula, Goa

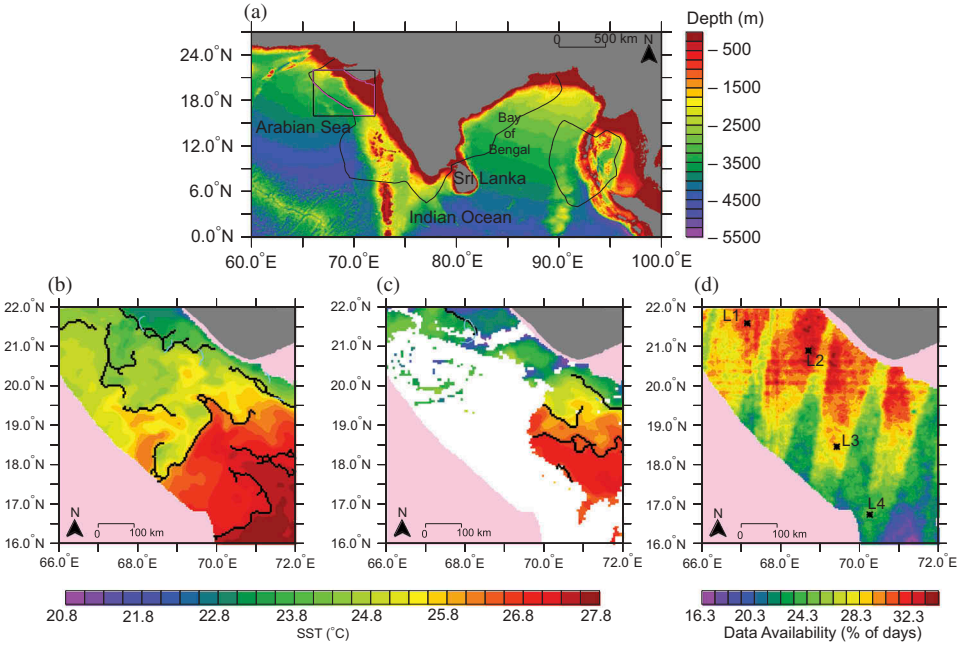

Figure 1. (a) Map of the north Indian Ocean, showing the region of interest. The black line denotes the EEZ of India. The model domain is the EEZ region in the rectangular black box in the northeastern Arabian Sea and is marked in pink coloured lines. (b) Satellite SST image illustrating the amount of data availability on 8 January 2014 (day is chosen as an example to represent the days on which the satellite data has negligible data gaps). The SST fronts are represented by the black lines and blue curves show the PFZs. The PFZ data are provided by ESSO-INCOIS (c) Same as (b) but for 11 January 2014, when the data gaps are huge and spread across almost half of the study region. (d) The number of days (in percentage) on which the SST data is available during 2013–2015. The asterisks denote the locations at which the observed and predicted SST timeseries are shown in Figure 5.

10 km in northeastern Arabian Sea (NEAS). In such applications, where high-resolution data are required, the data gaps are very detrimental.

One of the major reasons for the data gaps in the satellite data is the cloud cover, as infrared (IR) sensors (used to measure SST) cannot 'see' through the clouds (Wentz et al. 2000). The percentage of total cloud-free pixels for a time period from 1981 to 2011 shows that data availability is very low over the global oceans, with most of the regions showing less than 30% of cloud-free pixels (Obenour 2013). SSTs can also be measured using microwave radiations which can 'see' through the clouds (Wentz et al. 2000). But because of the low spatial resolution (about 25 km), these data can not be used for delineating fronts or PFZs, given the spatial scales of these oceanographic features are much less than 25 km (Deshpande, Radhakrishnan, and Bhat 2011).

The most commonly used method to tackle the problem of data gaps is to interpolate the data either in time or space. But the interpolation techniques over a large region (as is the case with data gaps because of the clouds) are in general very large, for example, see Figure 1(c) will lead to errors in the delineating PFZ advisories. Such errors could be reduced if one can predict the SST rather than using interpolation techniques (Pisoni,

Pastor, and Volta 2008). The prediction of SST would have an added advantage that it would be available in advance and could be used to improve the PFZ advisory services.

Given the importance for SST predictions, various methods have been proposed to predict SST along the course of time. The most commonly used methods are (i) numerical methods and (ii) statistical methods. The numerical methods make use of physical/chemical/biological parameters and complex inter-relationships among these variables to predict the SST of a region. Many authors have used coupled general circulation models (GCMs) to predict SST over a basin. For example, seasonal prediction of global SST anomalies using 13 state-of-the-art coupled global atmosphere–ocean models is presented by Krishnamurti et al. (2006). An analysis of the capabilities of the latest generation of coupled GCM seasonal forecast systems to predict tropical Atlantic SST anomalies is presented by Stockdale, Balmaseda, and Vidard (2006). Most widely used numerical models for the forecast of not just SST but a wide variety of parameters are the data assimilation and forecast systems developed by agencies such as European Centre for Medium-Range Weather Forecasts (ECMWF) and Command National Centers for Environmental Prediction (NCEP). ECMWF uses the Integrated Forecast System to give forecasts with a lead time of 10–15 days. The NCEP uses its Global Forecast Systems to give forecasts of various parameters 380 h ahead.

On the other hand, statistical methods range from simple extrapolation to complex methods like Markov model (Xue and Leetmaa 2000), regression (Kug et al. 2004), empirical canonical correlation (Collins, Reason, and Tangang 2004), and empirical orthogonal functions (Neetu et al. 2011) to predict SST. The statistical methods have the advantage that they are much lighter and easier to handle as it does not involve any complex physical mechanisms. Thus for predicting the SST on a smaller scale statistical methods are preferred to numerical methods. Some of these statistical techniques are being used to train artificial neural networks (ANNs) for better prediction.

The ANNs are efficiently being used as an alternative to statistical methods for different problems like estimation, classification, clustering analysis, sample recognition, feature extraction, etc. Since ANN models are usually nonlinear, these models give better estimates compared to linear statistical models such as autoregressive integrated moving average (Mammadov et al. 2006). ANN methods are more popular because of their flexibility in fitting to random data and their relatively simple development (Patil and Deo 2017). The ability of ANNs to sense out the trends and patterns in SST was recognized by the oceanographic community and was used by various researchers to predict SST at various spatial and temporal scales in world oceans. For example, Tangang, Hsieh, and Tang (1997) used ANN model to predict the seasonal SST variations over the selected regions in the tropical Pacific. Later Wu, Hsieh, and Tang (2006) used ANN for predicting the five leading principal components of SST over the tropical Pacific taking the sea-level pressure and SST anomalies as inputs. Garcia-Gorriz and Garcia-Sanchez (2007) analysed the ability of neural networks to estimate the seasonal and interannual SSTs in the western Mediterranean Sea from 1960 to 2005 using the monthly averages of meteorological parameters such as mean sea-level pressure, wind, temperature, and cloud cover.

ANNs were used by various authors to predict SST in the Indian Ocean. For example, Tripathi, Das, and Sahai (2006) used ANNs to assess the predictability of monthly SST anomalies averaged over region (27–35°N and 96–104°E) in the Indian Ocean. Patil et al. (2013) predicted the monthly mean of SST at six different locations in the North Indian

Ocean. Using a hybrid network called wavelet neural network, Patil, Deo, and Ravichandran (2016) predicted the SST anomalies over six different locations at three different timescales, daily, weekly, and monthly. The SST anomalies predicted at six locations by Patil et al. (2013) and Patil, Deo, and Ravichandran (2016) were not at exact (point) locations, but are small regions over which SST data were averaged, for example, in the Arabian Sea (19–20°N, 68°E), the Bay of Bengal (18–19°N, 90°E). The results showed that such neural networks were able to predict SST with a smaller error statistics compared to the numerical methods alone. A further study by Patil and Deo (2017) used wavelet neural network to predict SST at the selected (six) locations for 5 days in future.

However, all the above-mentioned studies in the Indian Ocean are either restricted to predicting SST at few locations or the SST values were averaged over a region. Unlike the earlier studies, our model considers both the spatial and temporal variability of SST in the selected region. Our model is trained with the SST spatial maps to predict SST over the selected region. For delineating SST fronts or PFZs, prediction of SST values over the entire region of interest is required, instead of a set of locations that take into consideration only temporal variability of SST at that particular location. The prediction of SST at selected locations without considering the SST variability in space is detrimental to the purpose of delineating SST fronts/PFZs. Hence, in the present study, we aim to develop an ANN model which considers the spatial variability of the SST along with the temporal variability.

The ANN model to predict SST was developed as a part of interdisciplinary programme called 'OCEAN FINDER' to study SST fronts and the ecosystem dynamics in these fronts; we conducted a few cruises in the NEAS (Vipin et al. 2015; Roy et al. 2015). The NEAS also happens to be the region in the Indian exclusive economic zone (EEZ) with the least data gaps in the satellite data compared to the other regions in the north Indian Ocean (Obenour 2013) and has more frontal probability (Vipin et al. 2015).

Yet another task of the 'OCEAN FINDER' is to develop tools for delineating SST fronts even during cloudy days. Hence, we retained NEAS as our study region to predict daily SST with a lead time of 1 day. For this purpose, we use the SST data of the preceding day to generate SST maps for the day. The scope of the ANN model developed under this study is not only to predict the SST/SST map one day in advance, but also to use the predicted SST to delineate fronts/PFZs in the EEZ.

2. Data and methods

2.1. *The ANN model*

We used daily SST data from the mid-IR band of MODIS on board NASA Aqua satellite platform. The data were downloaded from NASA Earth Observing System Data and Information System Physical Oceanography Distributed Active Archive Center at the Jet Propulsion Laboratory. The spatial resolution of the data is 4 km. The SST data were used for the training and testing of the ANN model. The network presented in this work was developed using *R* software environment version 3.3.1 (R Core Team 2016). We used an inbuilt ANN function ' PCAnnet' from the package 'Classification and regression training' developed by Kuhn et al. (2016). The network is a feed-forward neural network with Quasi-Newton back-propagation algorithm; detailed description of this algorithm can be obtained from Nocedal and Wrigh (1999).

A neural network consists of interconnected neurons, each acting as an independent computational element. Typically, neurons are connected in layers, and signals travel from the first (input) to the last (output) layer, passing through a range of hidden layers between them. Basic information on neural networks can be obtained from Ripley (1996) and Venables and Ripley (2002). Here, we provide a brief description of the ANN model developed in this study.

The model consists of an input layer, one hidden layer, and an output layer as shown in Figure 2(a). The input layer consists of eight neurons corresponding to the input SST data at each of the eight outer pixels of a 3×3 spatial grid. The input grid points are shown in dark grey shade in Figure 2(b). The size of each grid is 4 km corresponding to the spatial resolution of the satellite SST data. The hidden layer contains five neurons, which is about 2/3 of the size of the input layer. The size of the hidden layer is chosen following Karsoliya (2012). The number of neurons in the hidden layer is a significant factor that contributes to the overall performance of the network. Too few neurons in the hidden layer will starve the network of the resource, while too many of them will tend to learn the noise along with the relationship (Tripathi, Das, and Sahai 2006). The third and last layer of the network is the output layer with one neuron. This corresponds to the centre pixel of the 3×3 SST data grid, but for the next day, at which the model predicts the SST (shown in light grey shade in Figure 2(b)).

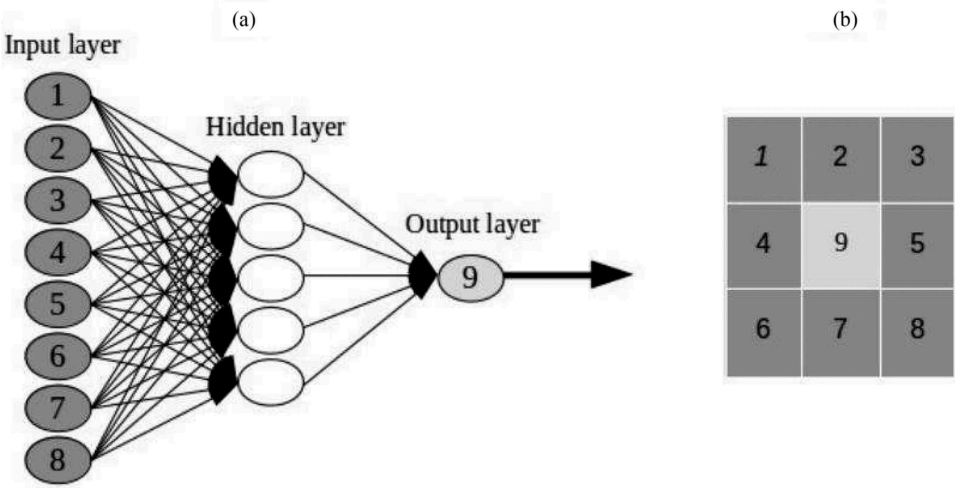

Figure 2. (a) A schematic diagram of the neural network showing input, hidden, and output layers. Circles filled in dark (light) grey represent the neurons in the input (output) layers. The hollow circles show the neurons in the hidden layer. (b) The 3×3 grid windows into which the model domain is divided. The eight outer pixels denoted by $1 - 8$ numbers represent the input pixels (dark grey shade). The SSTA data for the current day from these eight pixels are fed to the network shown in (a) as the input data. The centre pixel denoted by the number 9 represents the output (light grey shade) pixel. During training phase, SSTA data for the next day from the centre pixel are fed to network shown in (a) as a target output pixel. During prediction phase, the centre pixel is the output pixel, where the prediction is made.

2.2. *Data pre-processing*

The SST data are pre-processed to train the ANN. SST anomalies (SSTA) are estimated and then normalized. The normalized SSTA are used to train the network. Normalizing (or standardizing) the input data to the ANN is a common practice and is done to increase the processing speed and to reduce the chances of getting stuck in local optima (Dunne 2007).

2.2.1. *Estimation of SSTA*

To estimate SSTA, the model domain was divided into 3 × 3 grid windows (Figure 2(b)). The spatial SST mean at each pixel i is estimated from the surrounding eight pixels (indexed from 1 to 8, Figure 2(b)) as follows:

$$\overline{\mathrm{SST}}_{(i,k)} = \frac{1}{8}\sum_{i=1}^{8}(SST)_{(i,k)} \tag{1}$$

where $\mathrm{SST}_{(i,k)}$ corresponds to the SST at the each of the outer pixel of the 3 × 3 grid and the index i refers to the each of eight outer pixels and k represents the time index, corresponding to the current day. Then the spatial grid of 3 × 3 window is shifted in space such that the mean is estimated at each and every grid in the model domain on k day. To estimate the mean SST for the next day, k is then incremented by one and the mean is estimated in the entire spatial domain for $k + 1$ day and this method is repeated for all the days in 2013–2015.

After estimating the spatial mean, we calculate SSTA at each grid by subtracting the spatial SST mean of the eight pixels from the SST at that pixel and mathematically it can be represented as

$$SSTA_{(i,k)} = (SST)_{(i,k)} - \frac{1}{8}\sum_{i=1}^{8}(SST)_{(i,k)} \tag{2}$$

where $\mathrm{SST}_{(i,k)}$ and $\mathrm{SSTA}_{(i,k)}$ corresponds to the SST and SSTA respectively at the each of the outer pixel of the 3 × 3 grid and the index i refers to the each of eight outer pixels and k represents the time index, corresponding to the current day.

To estimate the SSTA at the centre pixel of the grid, where the model predicts the SST, the model will not have any information on the surrounding pixels and hence the SSTA at the centre pixel is estimated as

$$\mathrm{SSTA}_{(i=9,k+1)} = (SST)_{(i=9,k+1)} - \frac{1}{8}\sum_{i=1}^{8}(SST)_{(i,k)} \tag{3}$$

where $(k + 1)$ represents the next day and $i = 9$ represents the centre pixel. SSTA maps are generated by estimating SSTA at each and every pixel in the domain, by shifting the grid window in space.

The SSTA maps are then normalized with respect to time such that the normalized values have zero mean and unit variance. The formula to normalize is as follows:

$$SSTA_n = \frac{(SSTA) - (SSTA)_{min}}{(SSTA)_{\max} - (SSTA)_{\min}} \tag{4}$$

where $SSTA_n$ is the normalized SSTA, $SSTA_{max}$ is the maximum SSTA, and $SSTA_{min}$ is the minimum SSTA. The maximum and minimum values of SSTA are estimated at each location from the time series of the SSTA at that location. The normalized SSTA maps are then used to train the ANN.

2.3. *Training and testing of the ANN*

The training data set pattern is formed by combining the normalized data of the two days, the current day and the next day. The eight outer pixels of the 3×3 grid are fed with *SSTAn* of the current day as inputs and the centre pixel is fed with *SSTAn* of next day as target output. The training set includes the data in a particular grid if and only if the data are available at all the nine pixels of the grid (eight outer pixels for the current day data and one centre pixel for the next day). The training set excludes the grids that do not fulfil the criteria (data should be available at all nine pixels). Let us assume that per each day we get an n_k number of grids/patterns that satisfy the data availability criteria, where k index represents the time (in days). If n_k is less than say, P patterns (a cut-off for the maximum number of patterns), then the network picks up more patterns for the training from $k-1$, $k-2$ days, and so on till the number of patterns reaches a cut-off of 25,000 patterns. Hence, the number of days included in the training is subject to the data availability during the specified period. This flexibility of training dates is kept so that the ANN model converges for each training. The number of cycles/patterns used for training and testing the ANN is an important factor contributing to the performance of the ANN. If the training is stopped early, the network will not be able to converge and too long a training would lead to memorization of the training data (Tripathi, Das, and Sahai 2006). Hence, we chose a value of 25,000 patterns as the cut-off. This value of 25,000 patterns was arrived at after experimenting with the cut-off number with trial-and-error technique. However, a small change in the cut-off (say a few hundreds) did not effect the performance of the model. Of the data set picked up for the training and testing the ANN, the first 70% of the data is employed for training and the remaining 30% is for testing.

The training set thus generated is a single (training) set for our entire region of interest; this was done to capture the spatial variability and therefore our network is not site specific. However, to capture the temporal variability of SST, we changed our training every day, i.e. every day our network is trained with a new set of 25,000 patterns from its previous days. (An analogy to this type of training in terms of averaging is ' moving average' or 'running average'.)

2.4. *Prediction phase of ANN*

Once the network is trained by moving 'training method', the next step is to use this network for prediction. During the prediction phase, the inputs to the each of the windows of the trained network are the normalized SSTA at each of the eight outer pixels of the current day and the value at the centre pixel is predicted by the network for the next day. The output is then de-normalized to get the SSTA, and the average SST of that centre pixel on the previous day is added back to obtain the predicted SST at the centre pixel. Mathematically it can represented as

$$SST_{(i=9,k+1)} = (SSTA)_{(i=9,k+1)} + \frac{1}{8}\sum_{i=1}^{8}(SST)_{(i,k)} \tag{5}$$

where $(k+1)$ represents the day of prediction and $i = 9$ represents the centre pixel and $i =$ 1 to 8 represents the eight outer pixels of 3×3 grid of Figure 2(b).

For example, to predict the SST map on 10 January 2014 $(k+1)$ day, the model is trained using 25,000 samples available till 8 January 2014 $(k-1)$ day as shown in Figure 3. For prediction, the input normalized SSTA data to the trained model are given at eight outer pixels on 9 January 2014 (k) day and the output is predicted at the centre pixel on 10 January 2014 $(k+1)$ day as shown in Figures 2(b) and 3. Once all the possible data for 10 January 2014 are predicted, the SST maps are generated.

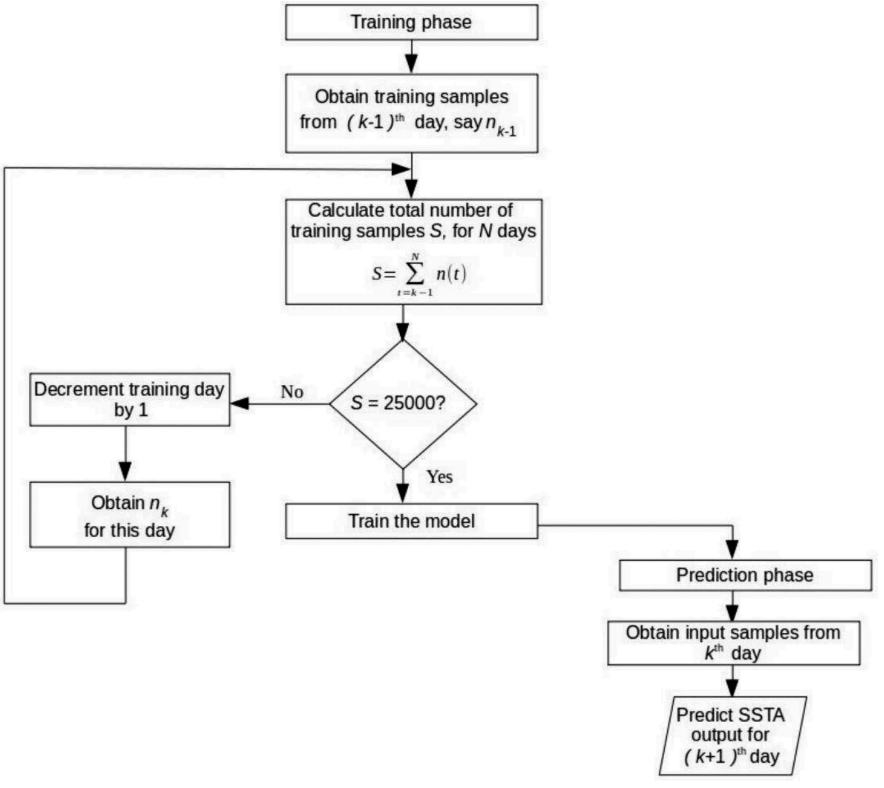

Figure 3. Illustration of the method of training of ANN model to predict SSTA on $(k+1)$th day. Say $(k+1)$ is the day on which SST is to be predicted. We take SSTA data from $k-2, k-3, k-4\ldots$. so on days, till the number of patterns equal 25,000. In the prediction phase, SSTA data are taken from eight outer pixels for $k-1$ day as shown in Figure 2(a) and the prediction is done at centre pixel on k day.

2.5. Validation of ANN output

The performance of the model is evaluated by two statistical error criteria: (i) root mean square error (RMSE) and (ii) mean absolute error at only those locations where satellite SST data are available on the prediction day.

3. Results

We used the ANN model to predict the daily SST (one day in advance) for a period of 3 years (from January 2013 till December 2015). In order to analyse the model error and enable comparison of the model results with observations, the prediction at a particular location was avoided if the satellite data were not available at that location on the day of prediction.

Figure 4 shows the comparison between the observed and predicted SST for a day in each of the year (2013–2015). The days are taken as example to show the performance of the model and are chosen, when the maximum satellite data are available on the prediction day. Along with the SST maps, the SST fronts are also marked for predicted and observed data. SST fronts are delineating using the algorithm of Cayula and Cornillon (1992) and the parameters are set in the SST front delineating algorithm following Vipin et al. (2015).

The model predicts all the major features of the SST variability reasonably well although there are slight differences. For example, during all the three days shown, low (warm) temperatures are observed in the northern (southern) region, which are well captured by the model. The low temperatures (<24.0°C) observed on 20 January 2014 in the northern region are predicted by the model. On 30 March 2013, in the southern region warm temperatures (about 28.0°C) are seen in both the observation and the model SST maps. On 15 February 2015, when the waters are at intermediate temperatures (25.0–27.0°C), SSTs are well captured by the model (Figure 4(a–f)).

SST fronts delineated on both the predicted and observed SST also well-matched. The SST fronts are the boundaries between the warm and cold waters. The horizontal temperature gradients are high in these zones. The frontal zones are predicted well by the model, though there are some minor differences between the observed and predicted SST fronts. For example, on 30 March 2013 a few short length SST fronts are seen in the predicted SST that are not present in the observed data. On 20 January 2014, one front at 66–67°E extended till 21.75°N in the observation, whereas the model could predict the front only till about 20.75°N. In the same region on 15 February 2015, the model could not capture a short-length SST front (Figure 4(j–l)). Apart from these minor differences, the model could predict all the SST fronts with reasonably less ambiguity.

But to give a quantitative parameter to measure the performance of the model, we estimate the difference between the observed SST and measured SST (error) at each pixel. $\varepsilon = (SST)_{\text{obs}} - (SST)_{\text{pre}}$ where ε is the error in the prediction and SST_{obs} and SST_{pre} are the observed and predicted values of SST, respectively. The error varies in the range of $\pm$ 0.5°C for most cases. However, there are small regions/pockets of high error where the magnitude of error is about $\pm$ 1.0°C. For example, near the coast on 30 March 2013 a negative high error (about −1.0°C) is observed and this high error also leads to a small

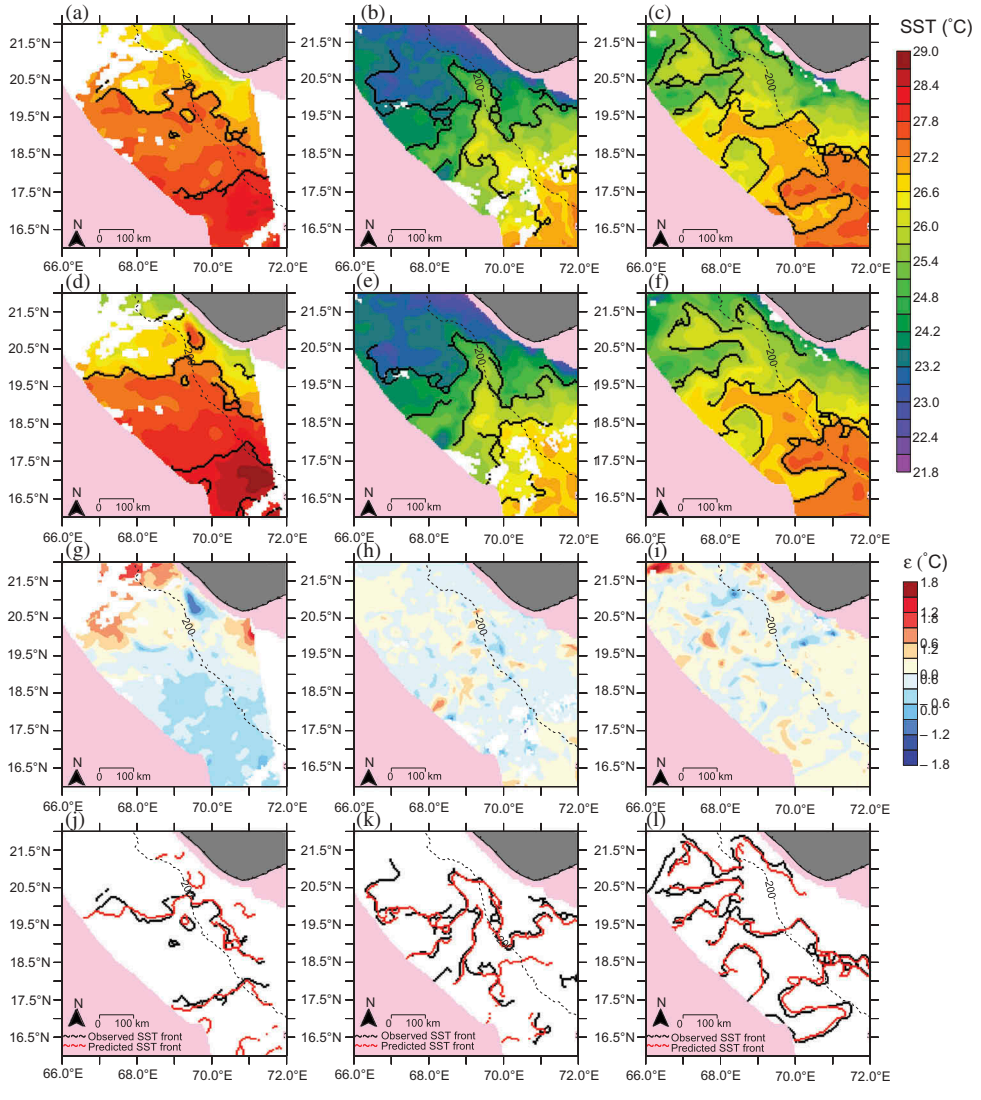

Figure 4. The performance of the model for 3 days on 30 March 2013, 20 January 2014, and 15 February 2015. Days are chosen as example (one day in each of the year). The SST values are plotted only in the EEZ region, the region outside EEZ is shaded in pink. Land is shaded in grey. The black dotted line shows the 200 m depth contour. The SST fronts are delineated and marked in black curves. Panels (a)–(c) show the spatial satellite SST maps for 3 days on 30 March 2013, 20 January 2014, and 15 February 2015, respectively. Panels (d)–(f) are same as (a)–(c) but for predicted SST maps for 3 days on 30 March 2013, 20 January 2014, and 15 February 2015, respectively. Panels (g)–(i) show the error (observed SST – predicted SST) in prediction maps for the 3 days on 30 March 2013, 20 January 2014, and 15 February 2015, respectively. Red colour (positive error) indicates that the model is under predicting, and the blue colour (negative error) indicates that the model is over predicting. Panels (j)–(l) show SST fronts drawn from observed (predicted) SST maps are in black (red) colour lines.

non-existent SST front in the predicted data. Similarly at (66ºE, 21.75ºN) on 15 February 2015, a high positive error patch is observed (Figure 4(g–i)).

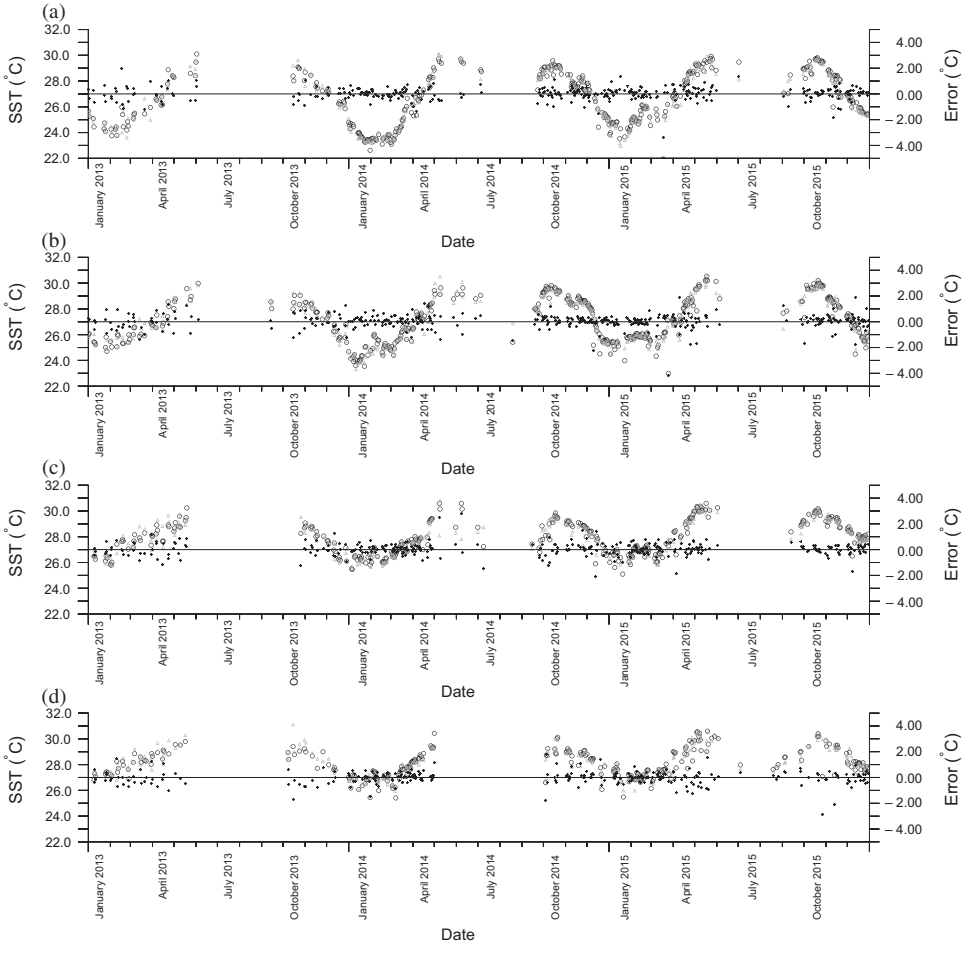

Figure 5. The time series of observed and predicted SST at four different locations L1, L2, L3, and L4 are plotted in (a), (b), (c), and (d), respectively. These locations are shown in Figure 1(d). Observed and predicted SST time series are plotted in black circles and grey triangles, respectively. The difference (error) between these two time series is plotted in small black dots in (a), (b), (c), and (d), respectively, for L1, L2, L3, and L4 locations. The positive (negative) error indicates the model is under (over) predicting SST.

The predicted spatial SST maps in Figure 4 show the performance of model in the entire model domain, but only for a few days. To show that the model's good performance is not restricted to only those few days, we plot the time series of predicted and observed SST for 3 years at a few selected locations (Figure 5). Locations are chosen, where more data are available and also care was taken such that these locations do not cluster in a small region, but scattered over the entire domain (Figure 1(d)). At any location, the maximum percentage of the data available is about 35% during 2013–2015. The data available at these four locations varies from 24% to 31%. During the summer monsoon (June–September) the data are not available at these locations also. The predicted and observed SST match well at these locations for all the three years. At locations L1 and L2, the minimum temperatures observed during the winter (December–

February) are as low as 22.0–23.0°C. At L3 and L4, the minimum values observed are 26.0°C. These minimum values are predicted well by the model. The maximum temperatures of 30.0°C during May at all these locations are predicted well by the model. The errors in the prediction are about ± 0.5°C for most of the time at all these locations, expect for a few days. One such case is seen in location L2 on 25 March 2015, when the SST falls well below 23.0°C.

3.1. *Error analysis*

Though the time series of the predicted SST and the error shows the performance of the model for the three years, it is restricted to only a few locations (Figure 5). Hence to quantitatively evaluate the performance of the model in the spatial and temporal domain and to check the accuracy of the prediction, we look into the RMSE for the entire spatial domain for each day. RMSE is estimated as follows:

$$RMSE = \sqrt{\frac{\sum_{i=1}^{N} ((SST)_{obs} - (SST)_{pre})^2}{N}} \tag{6}$$

where SST_{obs} and SST_{pre} are the observed and the predicted SST, respectively, N is the number of grid points/pixels, where the data are available on a particular day.

The RMSE for the three years are shown in Figure 6. The error ranges from 0.2°C to 1.0°C for most of the days. It is to be noted here that the RMSE is the error averaged over the entire spatial domain, and hence a lower error indicates that the error is low at all pixels on that day, but even small pockets of high error (as seen in the Figure 4(g,i)) would impact the RMSE value. Most of the days, the RMSE is clustered around 0.5°C. However, on some days, for example, on 17 December 2014 and 25 March 2015, we observe, high errors of about 2.0°C.

3.1.1. *Error distribution*

To assess the performance of the model, we need to assess the frequency of occurrence of these high error pockets, either in space (as seen in Figure 4(g,i)) or sudden short

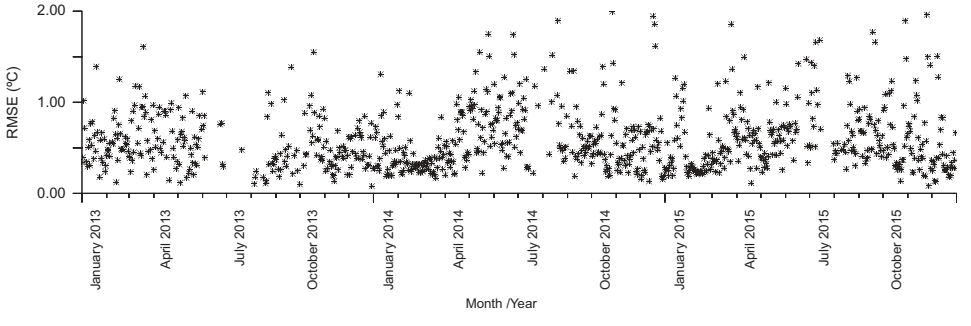

Figure 6. The daily mean RMSE from 2013–2015. The error is estimated for the entire spatial domain of the model. The days on which the data are available at less than 100 pixels are excluded from the estimation of RMSE.

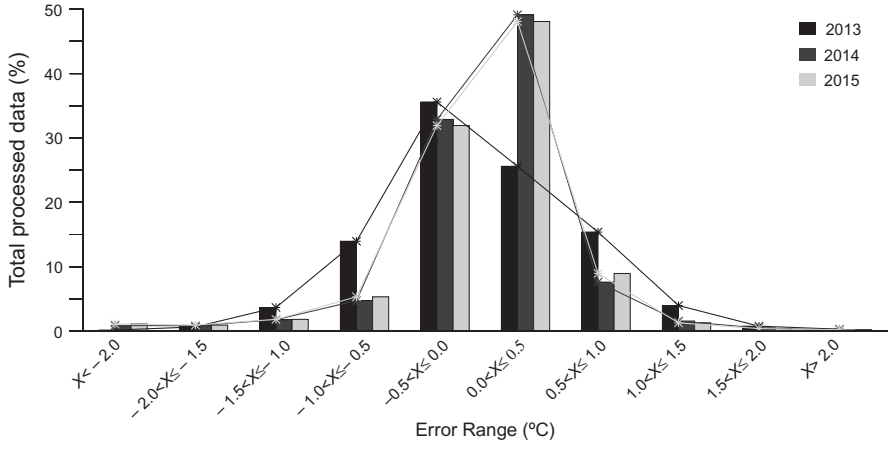

Figure 7. A bar chart showing the distribution of error for years 2013 (black bar), 2014 (dark grey bar), and 2015 (light grey bar). The abscissa is grouped into 10 error ranges (−0.5–0.0, 0.0–0.5, and so on) with a step size of 0.5°C error. The error ranges are open (closed) intervals at the lower (higher) end. The *y*-axis represents the percentage of total predictions corresponding to each of the error range group. The height of bar represents the number of prediction per hindered with the error lying in corresponding to error range in abscissa. The curved lines show the height of the coloured bars.

bursts in the error of prediction (as seen in Figure 5(b)). Hence, we use the distribution of the error (SST*obs* − SST*pre*) instead of the RMSE; the error distribution follows a skewed Gaussian curve (Figure 7). During 2014 and 2015 (2013), more than 80% (60%) of the model predictions has error $\leq \pm$ 0.5°C. For all the years under consideration more than 90%, the error values are $\leq \pm$ 1.0°C and the high errors of about 2.0°C in prediction occurred only around 1% of the total predictions.

3.1.2. *Monthwise error analysis*

We look at monthly absolute errors to evaluate the performance of the model during each month. During the summer monsoon, the data are sparsely available because of the clouds. The absolute errors values are also slightly higher during the monsoon months, particularly during June and July. During non-monsoon (monsoon) months the errors less than 0.5°C occurred around 70–80% (40–50%) of the model predictions and the absolute error values in the range 0.5–1.0°C occurred around 10–20% (30–40%) for non-monsoon (monsoon) months (Figure 8).

4. Discussion

One of the strengths of the ANN model set-up in the present study is its simplicity and its requirements; the only input it requires is the SST data from the previous 10–15 days. During monsoon months, the number of days increases to around 25–30 days. This simple data requirement makes this model much lighter and faster compared to the other methods. For example, Patil, Deo, and Ravichandran (2016) and Patil and Deo (2017) used huge amount of data (reanalysis, in situ and numerical data) and also used complex numerical methods for training the model.

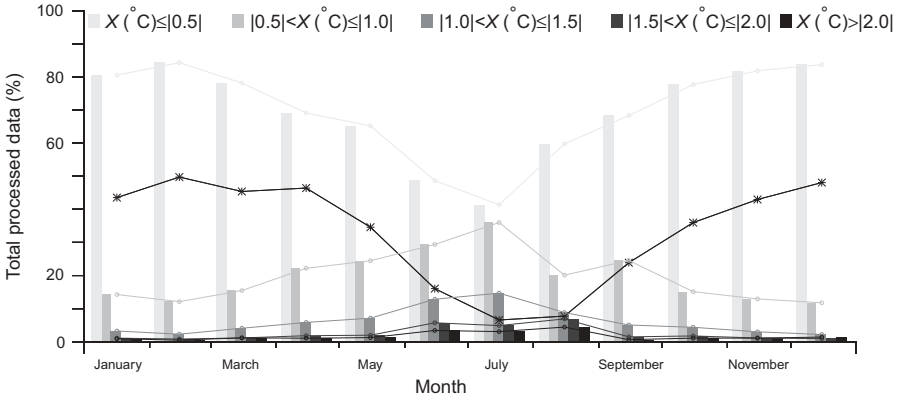

Figure 8. Bar chart showing the monthly error distribution during the period 2013–2015. The different shades of grey represent the different error ranges. The lightest shade denotes lowest error ($\leq |0.5|^{\circ}$C), and the darkest shade denotes highest error ($>|2.0|^{\circ}$C). The absolute error is taken to estimate the total percentage of the prediction in that error range. The black line shows the percentage of the data availability. The curved lines show the height of the coloured bars.

The second advantage of our model is that it is not site specific. We train the network by using spatial SST maps and not pixel by pixel. Unlike the models of Patil, Deo, and Ravichandran (2016) and Patil and Deo (2017), where the training changes from site to site depending on the time series of the SST at that location, our model is not site specific.

The third and the most significant strength of this model is that it considers both spatial and temporal variability of the SST for better prediction. The present model's network is trained with spatial SST maps to retain the spatial variability and the temporal variability is put into the model by varying SST maps on each and every day. But, the earlier studies, which used ANN to predict SST in the Indian Ocean, either averaged the SST over a region (Patil, Deo, and Ravichandran 2016), thereby ignoring the spatial variability of SST or considered point locations without considering the spatial variability (Patil and Deo 2017).

The merit of our ANN model is that it predicts the daily SST. The daily SST data is more volatile and random compared to monthly SST or the SST averaged over a region. The slow changing seasonal and trend components of a signal are easier to predict compared to fast varying signals. Some of the earlier studies used ANN to predict the seasonal and monthly SST (Tripathi, Das, and Sahai 2006; Patil et al. 2013). Given the highly volatile nature of the SST parameter and the shorter time and spatial scales of SST fronts in NEAS, the model performance is reasonably good. Our model tends to retain the SST gradients and is also able to pick the SST fronts reasonably well (Figure 4), which is the one of the aims of the study apart from predicting the SST. The errors involved in the prediction are in tolerable range $\pm 0.5^{\circ}$C for most of the predictions.

Though our model is designed with the significant merits mentioned above, it is not devoid of some limitations. Now, we present a brief review of the limitations of our model.

The performance of any model is dependent on the quality and quantity of the available input data. So the amount of the SST data available for training and prediction has an impact on the accuracy of the prediction. The present ANN model is designed such that it takes the

previous SST data over the region for training the network to ensure the convergence of the model. Thus while training the model, say, for example, during June or July, when the input data availability is less, the model gathers enough data from previous months like May. This leads to high errors in the prediction (Figure 8).

The data availability has another impact on our model. For the model to give prediction at a location, it has to have data in all the eight surrounding pixels (in a 3 × 3 grid window, Figure 2(b)) on the previous day. Failing this condition results in the location being left blank. The rigidity of this condition is a disadvantage leading to a large number of locations/pixels being left blank though they have data in nearby locations. This criterion is not a serious drawback if the data gaps extend over a larger area (as is the case with the data gaps of clouds which generally extend over a larger area). However, for shorter gaps, this rigid condition may prove to be a weakness of our model because every pixel is a part of nine adjacent 3 × 3 grid windows and thus leading to nine blanks in the prediction map.

Apart from the high errors in the prediction because of the data gaps, there are certain occasions when the model's prediction had high error, for example, on 17 December 2014 (Figure 9), the SST decreased from 27.5°C to 23.0°C. The model could not capture these sudden changes in the SST. A similar case was observed on 25 March 2015 (Figure 5(b)).

In spite of data gaps being hindrance to the performance of our model (but similar is the case for other models), it could predict SST in the EEZ of NEAS for each day during 2013–2015 and the SST fronts could also be delineated, which are helpful in drawing the PFZ advisories. Though in this study we restrict to a small region, the model could be easily extended to other regions. And since the model requires only one input (i.e. SST data) for training and prediction of SST, it can easily be tuned to other ocean parameters such as sea-level, which is more robust and less volatile than SST.

5. Summary

In the present study, we set up an ANN model to predict SST a day in advance. We chose the EEZ of NEAS as our study region. The model is trained with normalized SST maps; the number of patterns used for each day's training is 25,000 patterns. The trained ANN

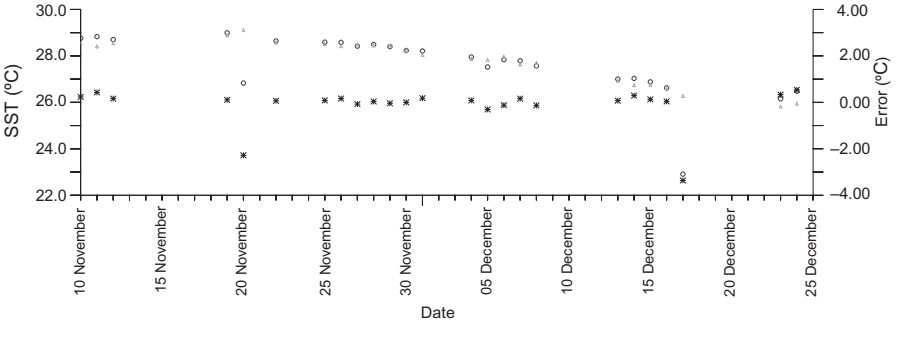

Figure 9. The observed (black circles) and predicted (grey triangles) time series of SST from 10 November till 31 December 2014 at location (70.5°E, 19.95°N). There is sharp decrease in observed temperature on 16 December. The right ordinate axis shows corresponding error time series in black asterisks. The model is not able to predict these sudden changes.

is then used for predicting the SST for the next day, using current day's SST maps. We used the model to predict (one day in advance) the spatial maps for the all the days during 2013–2015, and SST fronts were delineated. The error in the prediction is $< \pm$ 0.5°C for most of the predictions.

Acknowledgements

This study was funded by the OCEAN FINDER (PSC 0105) programmer of CSIR-NIO. We thank Dr D. Shankar for his constant encouragement, useful discussions and also for providing guidance at various stages of this work. We thank Mr Kankan Sarkar for SST delineating algorithm. We thank Mr Amol Kamble for helping us in writing a code to extract the EEZ region from the ocean basin. EEZ data is downloaded from http://iomenvis.nic.in. We acknowledge the help from Ms Remya, Mr P. Vipin, Mr S. Dora, and Mr Rahul Khedekar for plotting graphics and downloading SST satellite data. All plots are made using Ferret software. N. B. Arjun and Selrina D'Souza acknowledge MoES-INCOIS for the financial support. This is CSIR-NIO contribution 6189.

Disclosure statement

No potential conflict of interest was reported by the authors.

Funding

This study was funded by the OCEAN FINDER (PSC 0105) programmer of CSIR-NIO. N. B. Arjun and Selrina D'Souza acknowledge MoES-INCOIS for the financial support.

References

Cayula, J. F., and P. C. Cornillon. 1992. "Edge Detection Algorithm for SST Images." *Journal of Atmospheric and Oceanic Technology* 9: 67–80. doi:10.1175/1520-0426(1992)009<0067:EDAFSI>2.0.CO;2.

Collins, D. C., C. J. C. Reason, and F. Tangang. 2004. "Predictability of Indian Ocean Sea Surface Temperature Using Canonical Correlation Analysis." *Climate Dynamics* 22 (5): 481–497. doi:10.1007/s00382-004-0390-4.

Deshpande, S. P., K. V. Radhakrishnan, and U. G. Bhat. 2011. "Direct and Indirect Validation of Potential Fishing Zone Advisory off the Coast of Uttara Kannada, Karnataka." *Journal of the Indian Society of Remote Sensing* 39 (4): 547–554. doi:10.1007/s12524-011-0104-4.

Dunne, R. A. 2007. *A Statistical Approach to Neural Networks for Pattern Recognition (Wiley Series in Computational Statistics)*. New Jersey, NJ: Wiley-Interscience. ISBN 0471741086.

Garcia-Gorriz, E., and J. Garcia-Sanchez. 2007. "Prediction of Sea Surface Temperatures in the Western Mediterranean Sea by Neural Networks Using Satellite Observations." *Geophysical Research Letters* 34 (11). doi:10.1029/2007GL029888.

Karsoliya, S. 2012. "Approximating Number of Hidden Layer Neurons in Multiple Hidden Layer BPNN Architecture." *International Journal of Engineering Trends and Technology* 3 (6): 714–717. ISSN 2231-5381.

Krishnamurti, T. N., A. Chakraborty, R. Krishnamurti, W. K. Dewar, and C. A. Clayson. 2006. "Seasonal Prediction of Sea Surface Temperatures Anomalies Using a Suite of 13 Coupled Atmosphere-Ocean Models." *Journal of Climate* 19: 6069–6088. doi:10.1175/JCLI3938.1.

Kug, J.-S., I.-S. Kang, J.-Y. Lee, and J.-G. Jhun. 2004. "A Statistical Approach to Indian Ocean Sea Surface Temperature Prediction Using A Dynamical ENSO Prediction." *Geophysical Research Letters* 31 (9). doi:10.1029/2003GL019209.

Kuhn, M., J. Wing, S. Weston, A. Williams, C. Keefer, A. Engelhardt, T. Cooper, et al. 2016. *Caret: Classification and Regression Training*. R package version 6.0-71.

Mammadov, M., B. Yazici, S. Yolacan, A. Aslanargun, A. F. Yuzer, and E. Agaoglu. 2006. "Statistical Methods and Artificial Neural Networks." *Journal of Modern Applied Statistical Methods* 5: 495–512. doi:10.22237/jmasm/1162354980.

Neetu, F., R. Sharma, S. Basu, A. Sarkar, and P. K. Pal. 2011. "Data-Adaptive Prediction of Sea-Surface Temperature in the Arabian Sea." *IEEE Geoscience and Remote Sensing Letters* 8 (1): 9–13. doi:10.1109/LGRS.2010.2050674.

Nocedal, J., and S. J. Wrigh. 1999. *Numerical Optimization*. 1st ed. New York: Springer. ISBN 0-387-98793-2.

Obenour, K. M. 2013. "Temporal Trends in Global Sea Surface Temperature Fronts." Open Access Master's Thesis 59.

Patil, K., and M. C. Deo. 2017. "Prediction of Daily Sea Surface Temperature Using Efficient Neural Networks." *Ocean Dynamics* 67: 357–368. doi:10.1007/s10236-017-1032-9.

Patil, K., M. C. Deo, S. Ghosh, and M. Ravichandran. 2013. "Predicting Sea Surface Temperatures in the North Indian Ocean with Nonlinear Autoregressive Neural Networks." *International Journal of Oceanography* 2013: 1–11. doi:10.1155/2013/302479.

Patil, K., M. C. Deo, and M. Ravichandran. 2016. "Prediction of Sea Surface Temperature by Combining Numerical and Neural Techniques." *Journal of Atmospheric and Oceanic Technology* 33 (8): 1715–1726. doi:10.1175/JTECH-D-15-0213.1.

Pisoni, E., F. Pastor, and M. Volta. 2008. "Artificial Neural Networks to Reconstruct Incomplete Satellite Data: Application to the Mediterranean Sea Surface Temperature." *Nonlinear Processes in Geophysics* 15: 61–70. doi:10.5194/npg-15-61-2008.

R Core Team. 2016. *R: A Language and Environment for Statistical Computing*. Vienna, Austria: R Foundation for Statistical Computing.

Ripley, B. D. 1996. *Pattern Recognition and Neural Networks*. Cambridge, UK: Cambridge University Press.

Roy, R., R. Chitari, V. Kulkarni, M. S. Krishna, V. V. S. S. Sarma, and A. C. Anil. 2015. "CHEMTAX-derived Phytoplankton Community Structure Associated with Temperature Fronts in the Northeastern Arabian Sea." *Journal of Marine Systems* 144: 81–91. ISSN 0924-7963. doi:10.1016/j.jmarsys.2014.11.009.

Solanki, H. U., R. M. Dwivedi, S. R. Nayak, J. V. Jadeja, D. B. Thakar, H. B. Dave, and M. I. Patel. 2001. "Application of Ocean Colour Monitor Chlorophyll and AVHRR SST for Fishery Forecast: Preliminary Validation Results off Gujarat Coast, Northwest Coast of India." *Indian Journal of Marine Science* 30: 132–138.

Solanki, H. U., P. C. Mandoki, S. R. Nayak, and V. S. Somvanshi. 2005. "Evaluation of Remote-Sensing-Based Potential Fishing Zones (PFZS) Forecast Methodology." *Continental Shelf Research* 25: 2163–2173. doi:10.1016/j.csr.2005.08.025.

Stockdale, T. N., M. A. Balmaseda, and A. Vidard. 2006. "Tropical Atlantic SST Prediction with Coupled Ocean–Atmosphere GCMs." *Journal of Climate* 19: 6047–6061. doi:10.1175/JCLI3947.1.

Tangang, F. T., W. W. Hsieh, and B. Tang. 1997. "Forecasting the Equatorial Pacific Sea Surface Temperatures by Neural Network Models." *Climate Dynamics* 13: 135–147. doi:10.1007/s003820050156.

Tripathi, K. C., I. M. L. Das, and A. K. Sahai. 2006. "Predictability of Sea Surface Temperature Anomalies in the Indian Ocean Using Artificial Neural Networks." *Indian Journal of Marine Sciences* 35: 210–220.

Venables, W. N., and B. D. Ripley. 2002. *Modern Applied Statistics with S*. 4th ed. New York: Springer. ISBN 0-387-95457-0.

Vipin, P., K. Sarkar, S. G. Aparna, D. Shankar, V. V. S. S. Sarma, D. G. Gracias, M. S. Krishna, et al. 2015. "Evolution and Sub–Surface Characteristics of a Sea–Surface Temperature Filament and Front in the Northeastern Arabian Sea during November–December 2012." *Journal of Marine Systems* 150: 1–11. doi:10.1016/j.jmarsys.2015.05.003.

Wentz, F. J., C. Gentemann, D. Smith, and D. Chelton. 2000. "Satellite Measurements of Sea Surface Temperature through Clouds." *Science* 288 (5467): 847–850. doi:10.1126/science.288.5467.847.

Wu, A., W. W. Hsieh, and B. Tang. 2006. "Neural Network Forecasts of the Tropical Pacific Sea Surface Temperatures." *Neural Networks* 19 (2): 145–154. doi:10.1016/j.neunet.2006.01.004.

Xue, Y., and A. Leetmaa. 2000. "Forecasts of Tropical Pacific SST and Sea Level Using a Markov Model." *Geophysical Research Letters* 27 (17): 2701–2704. doi:10.1029/1999GL011107.

Zainuddin, M., S. I. Saitoh, and K. Saitoh. 2004. "Detection of Potential Fishing Ground for Albacore Tuna Using Synoptic Measurements of Ocean Color and Thermal Remote Sensing in the Northwestern North Pacific." *Geophysical Research Letters* 31 (20). doi:10.1029/2004GL021000.